

A Quasi-Wasserstein Loss for Learning Graph Neural Networks

Minjie Cheng^{1*} Hongteng Xu^{1,2*}

¹Gaoling School of Artificial Intelligence, Renmin University of China

²Beijing Key Laboratory of Big Data Management and Analysis Methods
chengminjie@ruc.edu.cn hongtengxu@ruc.edu.cn

March 14, 2024

Abstract

When learning graph neural networks (GNNs) in node-level prediction tasks, most existing loss functions are applied for each node independently, even if node embeddings and their labels are non-i.i.d. because of their graph structures. To eliminate such inconsistency, in this study we propose a novel Quasi-Wasserstein (QW) loss with the help of the optimal transport defined on graphs, leading to new learning and prediction paradigms of GNNs. In particular, we design a “Quasi-Wasserstein” distance between the observed multi-dimensional node labels and their estimations, optimizing the label transport defined on graph edges. The estimations are parameterized by a GNN in which the optimal label transport may determine the graph edge weights optionally. By reformulating the strict constraint of the label transport to a Bregman divergence-based regularizer, we obtain the proposed Quasi-Wasserstein loss associated with two efficient solvers learning the GNN together with optimal label transport. When predicting node labels, our model combines the output of the GNN with the residual component provided by the optimal label transport, leading to a new transductive prediction paradigm. Experiments show that the proposed QW loss applies to various GNNs and helps to improve their performance in node-level classification and regression tasks. The code of this work can be found at https://github.com/SDS-Lab/QW_Loss.

1 Introduction

Graph neural network (GNN) plays a central role in many graph learning tasks, such as social network analysis (Qiu et al. 2018, Fan et al. 2019, Zhang et al. 2023), molecular modeling (Satorras et al. 2021, Jiang et al. 2021, Wang et al. 2022), transportation forecasting (Wang et al. 2020, Li and Zhu 2021), and so on. Given a graph with node features, a GNN embeds the graph nodes by exchanging and aggregating the node features, whose implementation is based on message-passing operators in the spatial domain (Niepert et al. 2016, Kipf and Welling 2017, Veličković et al. 2018) or graph filters in the spectral domain (Defferrard et al. 2016, Chien et al. 2021, Bianchi et al. 2021, He et al. 2021). When some node labels are available, we can learn the GNN in a node-level semi-supervised learning (Yang et al. 2016, Kipf and Welling 2017, Xu et al. 2019c), optimizing the node embeddings to predict the observed labels. This learning framework has achieved encouraging performance in many node-level prediction tasks, e.g., node classification (Sen et al. 2008, McAuley et al. 2015).

*The two authors have equal contribution and are listed in the alphabetical order of their last names. Hongteng Xu is the corresponding author of this work.

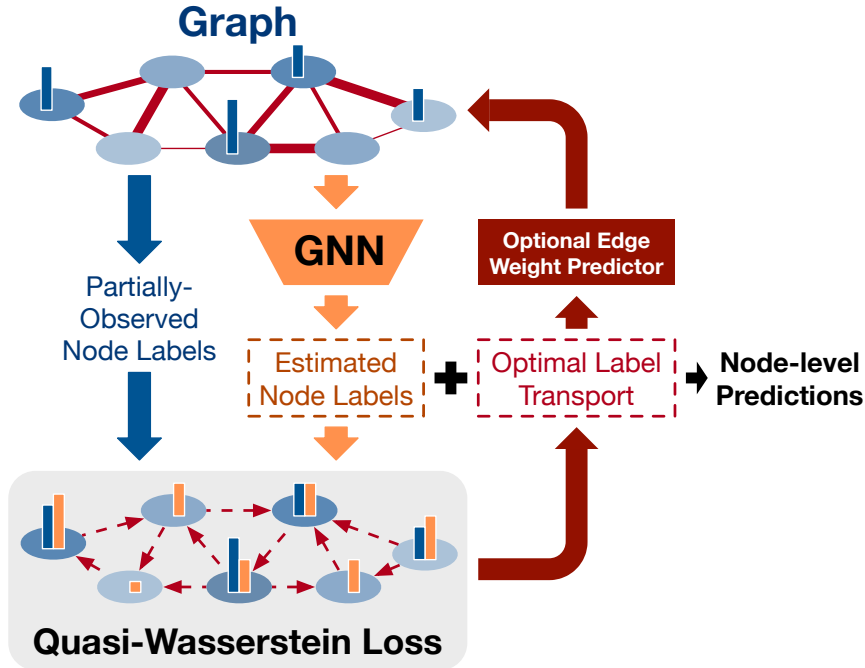


Figure 1: The scheme of our QW loss and the corresponding learning paradigm. Given a graph, whose node features are denoted as blue circles and partially-observed node labels are denoted as blue stems, a GNN embeds the nodes and estimates their labels (denoted as orange stems). By minimizing the QW loss, we obtain the optimal label transport (denoted as the dotted red arrows on edges) between the real and estimated node labels. Optionally, the optimal label transport determines the weights of graph edges (through an edge weight predictor). The final predictions are the combinations of the optimal label transport and the estimated node labels.

When applying the above node-level GNN learning framework, existing work often leverages a loss function (e.g., the cross-entropy loss) to penalize the discrepancy between each node’s label and the corresponding estimation. Here, some inconsistency between the objective design and the intrinsic data structure arises — the objective of learning a GNN is implemented as the summation of all the nodes’ loss functions, which is often applied for i.i.d. data, but the node embeddings and their labels are non-i.i.d. in general because of the underlying graph structure and the information aggregation achieved by the GNN. As a result, the current objective treats the losses of individual nodes independently and evenly, even if the nodes in the graph are correlated and have different significance for learning the GNN. Such inconsistency may lead to sub-optimal GNNs in practice, but to our knowledge none of existing work considers this issue in-depth.

To eliminate the inconsistency, we leverage computational optimal transport techniques (Peyré and Cuturi 2019), proposing a new objective called Quasi-Wasserstein (QW) loss for learning GNNs. As illustrated in Figure 1, given partially-observed node labels and their estimations parametrized by a GNN, we consider the optimal transport between them and formulate the problem as the aggregation of the Wasserstein distances (Frogner et al. 2015) corresponding to all label dimensions. This problem can be equivalently formulated as a label transport minimization problem (Essid and Solomon 2018, Facca and Benzi 2021) defined on the graph, leading to the proposed QW loss. By minimizing this loss, we can jointly learn the optimal label transport and the GNN parametrizing the label estimations. This optimization problem can be solved efficiently by Bregman divergence-

based algorithms, e.g., Bregman ADMM (Wang and Banerjee 2014, Xu 2020). Optionally, through a multi-layer perceptron (MLP), we can determine the edge weights of the graph based on optimal label transport, leading to a GNN with learnable edge weights.

The contributions of this study include the following two points:

- **A theoretically-solid loss without the inconsistency issue.** The QW loss provides a new optimal transport-based loss for learning GNNs, which considers the labels and estimations of graph nodes jointly. Without the questionable i.i.d. assumption, it eliminates the inconsistency issue mentioned above. In theory, we demonstrate that the QW loss is a valid metric for the node labels defined on graphs. Additionally, the traditional objective function for learning GNNs can be treated as a special case of our QW loss. We further demonstrate that applying our QW loss reduces data fitting errors in the training phase.
- **New learning and prediction paradigms.** Different from the existing methods that combine GNNs with label propagation mechanisms (Huang et al. 2021, Wang and Leskovec 2021, Dong et al. 2021), the QW loss provides a new way to combine node embeddings with label information in both training and testing phases. Bregman divergence-based algorithms are applied to learn the model, and the final model consists of the GNN and the optimal label transport. When predicting node labels, the model combines the estimations provided by the GNN with the complementary information from the optimal label transport, leading to a new transductive prediction paradigm.

Experiments demonstrate that our QW loss applies to various GNNs and helps to improve their performance in various node-level classification and regression tasks.

2 Related work

2.1 Graph Neural Networks

Graph neural networks can be coarsely categorized into two classes. The GNNs in the first class apply spatial convolutions to graphs (Niepert et al. 2016). The representative work includes the graph convolutional network (GCN) in (Kipf and Welling 2017), the graph attention network (GAT) in (Veličković et al. 2018), and their variants (Zhuang and Ma 2018, Wang et al. 2019, Fu et al. 2020). The GNNs in the second class achieve graph spectral filtering (Guo et al. 2023). They are often designed based on a polynomial basis, such as ChebNet (Defferrard et al. 2016) and its variants (He et al. 2022), GPR-GNN (Chien et al. 2021), and BernNet (He et al. 2021). Besides approximated by the polynomial basis, the spectral GNNs can be learned by other strategies, e.g., Personalized PageRank in APPNP (Gasteiger et al. 2019), graph optimization functions in GNN-LF/HF (Zhu et al. 2021), ARMA filters (Bianchi et al. 2021), and diffusion kernel-based filters (Klicpera et al. 2019, Xu et al. 2019c, Du et al. 2022). The above spatial and spectral GNNs are correlated because a spatial convolution always corresponds to a graph spectral filter (Balcilar et al. 2021). For example, GCN (Kipf and Welling 2017) can be explained as a low-pass filter achieved by a first-order Chebyshev polynomial. Given a graph with some labeled nodes, we often learn the above GNNs in a semi-supervised node-level learning framework (Kipf and Welling 2017, Yang et al. 2016), in which the GNNs embed all the nodes and are trained under the supervision of the labeled nodes. However, the objective functions used in the framework treat the graph nodes independently and thus mismatch with the non-i.i.d. nature of the data. To model label dependency, one implementation, like GMNN (Qu et al. 2019), enhances GNNs by modeling label distribution with a conditional random field based on node embeddings. Differently, our work

focuses on establishing a flow of label transformation along edges, compensating for prediction errors across various GNN models.

2.2 Computational Optimal Transport

As a powerful mathematical tool, optimal transport (OT) distance (or called Wasserstein distance under some specific settings) provides a valid metric for probability measures (Villani 2008), which has been widely used for various machine learning problems, e.g., distribution comparison (Frogner et al. 2015, Lee et al. 2019), point cloud registration (Grave et al. 2019), graph partitioning (Dong and Sawin 2020, Xu et al. 2019b), generative modeling (Arjovsky et al. 2017, Tolstikhin et al. 2018), and so on. Typically, the OT distance corresponds to a constrained linear programming problem. To approximate the OT distance with low complexity, many algorithms have been proposed, e.g., Sinkhorn-scaling (Cuturi 2013), Bregman ADMM (Wang and Banerjee 2014), Conditional Gradient (Titouan et al. 2019), and Inexact Proximal Point (Xie et al. 2020). Recently, two iterative optimization methods have been proposed to solve the optimal transport problems defined on graphs (Essid and Solomon 2018, Facca and Benzi 2021). These efficient algorithms make the OT distance a feasible loss for machine learning problems, e.g., the Wasserstein loss in (Frogner et al. 2015). Focusing on the learning of GNNs, the work in (Chen et al. 2020) proposes a Wasserstein distance-based contrastive learning method. The Gromovized Wasserstein loss is applied to learn cross-graph node embeddings (Xu et al. 2019b), graph factorization models (Vincent-Cuaz et al. 2021, Xu 2020), and GNN-based graph autoencoders (Xu et al. 2022). The above work is designed for graph-level learning tasks, e.g., graph matching, representation, classification, and clustering. Our QW loss, on the contrary, is designed for node-level prediction tasks, resulting in significantly different learning and prediction paradigms.

3 Proposed Method

3.1 Motivation and Principle

Denote a graph as $G(\mathcal{V}, \mathcal{E})$, where \mathcal{V} represents the set of nodes and \mathcal{E} represents the set of edges, respectively. The graph G is associated with an adjacency matrix $\mathbf{A} \in \mathbb{R}^{|\mathcal{V}| \times |\mathcal{V}|}$ and a edge weight vector $\mathbf{w} = [w_e] \in \mathbb{R}^{|\mathcal{E}|}$. The weights in \mathbf{w} correspond to the non-zero elements in \mathbf{A} . For an unweighted graph, \mathbf{A} is a binary matrix, and \mathbf{w} is an all-one vector. Additionally, the nodes of the graph may have D -dimensional features, which are formulated as a matrix $\mathbf{X} \in \mathbb{R}^{|\mathcal{V}| \times D}$. Suppose that a subset of nodes, denoted as $\mathcal{V}_L \subset \mathcal{V}$, are annotated with C -dimensional labels, i.e., $\{\mathbf{y}_v \in \mathbb{R}^C\}_{v \in \mathcal{V}_L}$. We would like to learn a GNN to predict the labels of the remaining nodes, i.e., $\{\mathbf{y}_v\}_{v \in \mathcal{V} \setminus \mathcal{V}_L}$.

The motivation for applying GNNs is based on the non-i.i.d. property of the node features and labels. Suppose that we have two nodes connected by an edge, i.e., $(v, v') \in \mathcal{E}$, where $(\mathbf{x}_v, \mathbf{y}_v)$ and $(\mathbf{x}_{v'}, \mathbf{y}_{v'})$ are their node features and labels. For each node, its neighbors' features or labels can provide valuable information to its prediction task, i.e., the conditional probability $p(\mathbf{y}_v | \mathbf{x}_v) \neq p(\mathbf{y}_v | \mathbf{x}_v, \mathbf{x}_{v'})$ and $p(\mathbf{y}_v | \mathbf{x}_v) \neq p(\mathbf{y}_v | \mathbf{x}_v, \mathbf{y}_{v'})$ in general. Similarly, for node pairs, their labels are often conditionally-dependent, i.e., $p(\mathbf{y}_v, \mathbf{y}_{v'} | \mathbf{x}_v, \mathbf{x}_{v'}) = p(\mathbf{y}_v | \mathbf{x}_v, \mathbf{x}_{v'}, \mathbf{y}_{v'}) p(\mathbf{y}_{v'} | \mathbf{x}_v, \mathbf{x}_{v'}) \neq p(\mathbf{y}_v | \mathbf{x}_v, \mathbf{x}_{v'}) p(\mathbf{y}_{v'} | \mathbf{x}_v, \mathbf{x}_{v'})$. More generally, for all node labels, we have

$$p(\{\mathbf{y}_v\}_{v \in \mathcal{V}} | \mathbf{X}, \mathbf{A}) \neq \prod_{v \in \mathcal{V}} p(\mathbf{y}_v | \mathbf{X}, \mathbf{A}), \quad (1)$$

Ideally, we shall learn a GNN to maximize the conditional probability of all labeled nodes, i.e., $\max p(\{\mathbf{y}_v\}_{v \in \mathcal{V}_L} | \mathbf{X}, \mathbf{A})$. In practice, however, most existing methods formulate the node-level

learning paradigm of the GNN as

$$\max_{\theta} \prod_{v \in \mathcal{V}_L} p(\mathbf{y}_v | \mathbf{X}, \mathbf{A}; \theta) \Leftrightarrow \min_{\theta} \sum_{v \in \mathcal{V}_L} \psi(g_v(\mathbf{X}, \mathbf{A}; \theta), \mathbf{y}_v). \quad (2)$$

Here, g is a graph neural network whose parameters are denoted as θ . Taking the adjacency matrix \mathbf{A} and the node feature matrix \mathbf{X} as input, the GNN g predicts the node labels. $g_v(\mathbf{X}, \mathbf{A}; \theta)$ represents the estimation of the node v 's label achieved by the GNN, which is also denoted as $\hat{\mathbf{y}}_v$. Similarly, we denote $g_{\mathcal{V}}(\mathbf{X}, \mathbf{A}; \theta)$ as the estimated labels for the node set \mathcal{V} in the following content. The loss function $\psi : \mathbb{R}^C \times \mathbb{R}^C \mapsto \mathbb{R}$ is defined in the node level. In node-level classification tasks, it is often implemented as the cross-entropy loss or the KL-divergence (i.e., $p(\mathbf{y}_v | \mathbf{X}, \mathbf{A}; \theta)$ is modeled by the softmax function). In node-level regression tasks, it is often implemented as the least-square loss (i.e., $p(\mathbf{y}_v | \mathbf{X}, \mathbf{A}; \theta)$ is assumed to be the Gaussian distribution).

The loss in (2) assumes the node labels to be conditionally-independent with each other, which may be too strong in practice and inconsistent with the non-i.i.d. property of graph-structured data shown in (1). To eliminate such inconsistency, we should treat node labels as a set rather than independent individuals, developing a set-level loss to penalize the discrepancy between the observed labels and their estimations globally, i.e.,

$$\min_{\theta} \text{Loss}(g_{\mathcal{V}_L}(\mathbf{X}, \mathbf{A}; \theta), \{\mathbf{y}_v\}_{v \in \mathcal{V}_L}). \quad (3)$$

In the following content, we will design such a loss with theoretical supports, based on the optimal transport on graphs.

3.2 Optimal Transport on Graphs

Suppose that we have two measures on a graph $G(\mathcal{V}, \mathcal{E})$, denoted as $\boldsymbol{\mu} \in [0, \infty)^{|\mathcal{V}|}$ and $\boldsymbol{\gamma} \in [0, \infty)^{|\mathcal{V}|}$, respectively. The element of each measure indicates the ‘‘mass’’ of a node. Assume the two measures to be balanced, i.e., $\langle \boldsymbol{\gamma} - \boldsymbol{\mu}, \mathbf{1}_{|\mathcal{V}|} \rangle = 0$, where $\langle \cdot, \cdot \rangle$ is the inner product operator. The optimal transport, or called the 1-Wasserstein distance (Villani 2008), between them is defined as

$$W_1(\boldsymbol{\mu}, \boldsymbol{\gamma}) := \min_{\mathbf{T} \in \Pi(\boldsymbol{\mu}, \boldsymbol{\gamma})} \langle \mathbf{D}, \mathbf{T} \rangle = \min_{\mathbf{T} \in \Pi(\boldsymbol{\mu}, \boldsymbol{\gamma})} \sum_{v, v' \in \mathcal{V} \times \mathcal{V}} t_{vv'} d_{vv'}, \quad (4)$$

where $\mathbf{D} = [d_{vv'}] \in \mathbb{R}^{|\mathcal{V}| \times |\mathcal{V}|}$ represents the shortest path distance matrix, and $\Pi(\boldsymbol{\mu}, \boldsymbol{\gamma}) = \{\mathbf{T} \geq \mathbf{0} | \mathbf{T} \mathbf{1}_{|\mathcal{V}|} = \boldsymbol{\mu}, \mathbf{T}^{\top} \mathbf{1}_{|\mathcal{V}|} = \boldsymbol{\gamma}\}$ represents the set of all valid doubly stochastic matrices. Each $\mathbf{T} = [t_{vv'}] \in \Pi(\boldsymbol{\mu}, \boldsymbol{\gamma})$ is a transport plan matrix. The optimization problem in (4) corresponds to finding the optimal transport plan $\mathbf{T}^* = [t_{vv'}^*]$ to minimize the ‘‘cost’’ of changing $\boldsymbol{\mu}$ to $\boldsymbol{\gamma}$, in which the cost is measured as the sum of ‘‘mass’’ $t_{vv'}$ moved from node v to node v' times distance $d_{vv'}$.

3.2.1 Wasserstein Distance for Vectors on A Graph

For the optimal transport problem defined on graphs, we can simplify the problem in (4) by leveraging the underlying graph structures. As shown in (Essid and Solomon 2018, Santambrogio 2015), given a graph $G(\mathcal{V}, \mathcal{E})$, we can define a sparse matrix $\mathbf{S}_{\mathcal{V}} = [s_{ve}] \in \{0, \pm 1\}^{|\mathcal{V}| \times |\mathcal{E}|}$ to indicating the graph topology. For node v and edge e , the corresponding element in $\mathbf{S}_{\mathcal{V}}$ is

$$s_{ve} = \begin{cases} 1 & \text{if } v \text{ is ‘‘head’’ of edge } e \\ -1 & \text{if } v \text{ is ‘‘tail’’ of edge } e \\ 0 & \text{otherwise.} \end{cases} \quad (5)$$

When G is directed, the “head” and “tail” of each edge are predefined. When G is undirected, we can randomly define each edge’s “head” and “tail” in advance. Accordingly, the 1-Wasserstein distance in (4) can be equivalently formulated as a minimum-cost flow problem:

$$W_1(\boldsymbol{\mu}, \boldsymbol{\gamma}) = \min_{\mathbf{f} \in \Omega(\mathbf{S}_{\mathcal{V}}, \boldsymbol{\mu}, \boldsymbol{\gamma})} \|\text{diag}(\mathbf{w})\mathbf{f}\|_1, \quad (6)$$

where $\text{diag}(\mathbf{w})$ is a diagonal matrix constructed by the edge weights of the graph. The vector $\mathbf{f} = [f_e] \in \Omega(\mathbf{S}_{\mathcal{V}}, \boldsymbol{\mu}, \boldsymbol{\gamma})$ is the flow indicating the mass passing through each edge. Accordingly, the cost corresponding to edge e is represented as the distance w_e times the mass f_e , and the sum of all the costs leads to the objective function in (6). The feasible domain of the flow vector is defined as

$$\Omega(\mathbf{S}_{\mathcal{V}}, \boldsymbol{\mu}, \boldsymbol{\gamma}) = \mathcal{U}^{|\mathcal{E}|} \cap \{\mathbf{f} \mid \mathbf{S}_{\mathcal{V}}\mathbf{f} = \boldsymbol{\gamma} - \boldsymbol{\mu}\}, \text{ where } \mathcal{U} = \begin{cases} [0, \infty), & \text{Directed } G, \\ \mathbb{R}, & \text{Undirected } G. \end{cases} \quad (7)$$

The constraint $\mathbf{S}_{\mathcal{V}}\mathbf{f} = \boldsymbol{\gamma} - \boldsymbol{\mu}$ ensures that the flow on all the edges leads to the change from $\boldsymbol{\mu}$ to $\boldsymbol{\gamma}$. The flow in the directed graph is nonnegative, which can only pass through each edge from “head” to “tail”. On the contrary, the undirected graph allows the mass to transport from “tail” to “head”. By solving (6), we find the optimal flow \mathbf{f}^* (or the so-called optimal transport on edges) that minimizes the overall cost $\|\text{diag}(\mathbf{w})\mathbf{f}\|_1$.

3.2.2 Partial Wasserstein Distance for Vectors on a Graph

When only a subset of nodes (i.e., $\mathcal{V}_L \subset \mathcal{V}$) have observable signals, we can define a *partial Wasserstein distance* on the graph by preserving the constraints relevant to \mathcal{V}_L : for $\boldsymbol{\mu}, \boldsymbol{\gamma} \in \mathbb{R}^{|\mathcal{V}_L|}$, we have

$$W_1^{(P)}(\boldsymbol{\mu}, \boldsymbol{\gamma}) = \min_{\mathbf{f} \in \Omega(\mathbf{S}_{\mathcal{V}_L}, \boldsymbol{\mu}, \boldsymbol{\gamma})} \|\text{diag}(\mathbf{w})\mathbf{f}\|_1, \quad (8)$$

where $\mathbf{S}_{\mathcal{V}_L} \in \{0, \pm 1\}^{|\mathcal{V}_L| \times |\mathcal{E}|}$ is a submatrix of $\mathbf{S}_{\mathcal{V}}$, storing the rows corresponding to the nodes with observable signals.

Different from the classic Wasserstein distance, the Wasserstein distance defined on graphs is not limited for nonnegative vectors because the minimum-cost flow formulation in (6) is *shift-invariant*, i.e., $\forall \boldsymbol{\delta} \in \mathbb{R}^{|\mathcal{V}|}$, $W_1(\boldsymbol{\mu}, \boldsymbol{\gamma}) = W_1(\boldsymbol{\mu} - \boldsymbol{\delta}, \boldsymbol{\gamma} - \boldsymbol{\delta})$. The partial Wasserstein distance in (8) can be viewed as a generalization of (6), and thus it holds the shift-invariance as well. Moreover, given an undirected graph, we can prove that both the W_1 in (6) and the $W_1^{(P)}$ in (8) can be valid metrics in the spaces determined by the topology of an undirected graph (See Appendix A for a complete proof).

Theorem 1 (Metric Property). *Given an undirected graph $G(\mathcal{V}, \mathcal{E})$, with edge weights $\mathbf{w} \in [0, \infty)^{|\mathcal{E}|}$ and a matrix $\mathbf{S}_{\mathcal{V}} \in \{0, \pm 1\}^{|\mathcal{V}| \times |\mathcal{E}|}$ defined in (5), the W_1 in (6) is a metric in $\text{Range}(\mathbf{S}_{\mathcal{V}})$, and the $W_1^{(P)}$ in (8) is a metric in $\text{Range}(\mathbf{S}_{\mathcal{V}_L})$, $\forall \mathcal{V}_L \in \mathcal{V}$.*

The flow vector \mathbf{f} in (8) has fewer constraints than that in (6), so the relation between W_1 and $W_1^{(P)}$ obeys the following theorem.

Theorem 2 (Monotonicity). *Given an undirected graph $G(\mathcal{V}, \mathcal{E})$, with edge weights $\mathbf{w} \in [0, \infty)^{|\mathcal{E}|}$ and a matrix $\mathbf{S}_{\mathcal{V}} \in \{0, \pm 1\}^{|\mathcal{V}| \times |\mathcal{E}|}$ defined in (5), we have*

$$W_1(\boldsymbol{\mu}, \boldsymbol{\gamma}) \geq W_1^{(P)}(\boldsymbol{\mu}_{\mathcal{V}'}, \boldsymbol{\gamma}_{\mathcal{V}'}) \geq W_1^{(P)}(\boldsymbol{\mu}_{\mathcal{V}''}, \boldsymbol{\gamma}_{\mathcal{V}''}) \geq 0, \quad \forall \boldsymbol{\mu}, \boldsymbol{\gamma} \in \text{Range}(\mathbf{S}_{\mathcal{V}}), \mathcal{V}'' \subset \mathcal{V}' \subset \mathcal{V}, \quad (9)$$

where $\boldsymbol{\mu}_{\mathcal{V}'}$ denotes the subvector of $\boldsymbol{\mu}$ corresponding to the set \mathcal{V}' .

3.3 Learning GNNs with Quasi-Wasserstein Loss

Inspired by the optimal transport on graphs, we propose a Quasi-Wasserstein loss for learning GNNs. Given a partially-labeled graph G , we formulate observed labels as a matrix $\mathbf{Y}_{\mathcal{V}_L} = [\mathbf{y}_{\mathcal{V}_L}^{(c)}] \in \mathbb{R}^{|\mathcal{V}_L| \times C}$, where $\mathbf{y}_{\mathcal{V}_L}^{(c)} \in \mathbb{R}^{|\mathcal{V}_L|}$ represents the labels in c -th dimension. The estimated labels generated by a GNN g are represented as $\widehat{\mathbf{Y}}_{\mathcal{V}_L} = [\widehat{\mathbf{y}}_{\mathcal{V}_L}^{(c)}] := g_{\mathcal{V}_L}(\mathbf{X}, \mathbf{A}; \theta)$. Our QW loss is defined as

$$\begin{aligned} QW(\widehat{\mathbf{Y}}_{\mathcal{V}_L}, \mathbf{Y}_{\mathcal{V}_L}) &= \sum_{c=1}^C W_1^{(P)}(\widehat{\mathbf{y}}_{\mathcal{V}_L}^{(c)}, \mathbf{y}_{\mathcal{V}_L}^{(c)}) \\ &= \sum_{c=1}^C \min_{\mathbf{f}^{(c)} \in \Omega(\mathbf{S}_{\mathcal{V}_L}, \widehat{\mathbf{y}}_{\mathcal{V}_L}^{(c)}, \mathbf{y}_{\mathcal{V}_L}^{(c)})} \|\text{diag}(\mathbf{w}) \mathbf{f}^{(c)}\|_1 \\ &= \min_{\mathbf{F} \in \Omega_C(\mathbf{S}_{\mathcal{V}_L}, g_{\mathcal{V}_L}(\mathbf{X}, \mathbf{A}; \theta), \mathbf{Y}_{\mathcal{V}_L})} \|\text{diag}(\mathbf{w}) \mathbf{F}\|_1, \end{aligned} \quad (10)$$

where $\mathbf{F} = [\mathbf{f}^{(c)}]$ is the flow matrix, and its feasible domain $\Omega_C = \mathcal{U}^{|\mathcal{E}| \times C} \cap \{\mathbf{F} | \mathbf{S}_{\mathcal{V}_L} \mathbf{F} = \mathbf{Y}_{\mathcal{V}_L} - g_{\mathcal{V}_L}(\mathbf{X}, \mathbf{A}; \theta)\}$. $W_1^{(P)}(\widehat{\mathbf{y}}_{\mathcal{V}_L}^{(c)}, \mathbf{y}_{\mathcal{V}_L}^{(c)})$ is the partial Wasserstein distance between the observed and estimated labels in the c -th dimension. The QW loss is the summation of the C partial Wasserstein distances, and it can be rewritten as the summation of C minimum-cost flow problems. As shown in the third row of (10), these C problems can be formulated as a single optimization problem, and the variables of the problems are aggregated as the flow matrix \mathbf{F} . Based on Theorem 1, our QW loss is a metric for the matrices whose columns are in $\text{Range}(\mathbf{S}_{\mathcal{V}_L})$.

The optimal flow matrix $\mathbf{F}^* = [\mathbf{f}^{(c)*}]$ is called **optimal label transport** in this study, in which the column $\mathbf{f}^{(c)*}$ indicating the optimal transport on graph edges between the observed labels and their estimations in the c -th dimension. Note that, we call the proposed loss ‘‘Quasi-Wasserstein’’ because *i*) it is not equal to the classic 1-Wasserstein distance between the label sets $\widehat{\mathbf{Y}}_{\mathcal{V}_L}$ and $\mathbf{Y}_{\mathcal{V}_L}$ (Peyré and Cuturi 2019), and *ii*) the optimal label transport \mathbf{F}^* cannot be reformulated as the optimal transport \mathbf{T}^* obtained by (4). When $\mathbf{F}^* = \mathbf{0}$, we have $QW(\widehat{\mathbf{Y}}_{\mathcal{V}_L}, \mathbf{Y}_{\mathcal{V}_L}) = 0$ and accordingly, $\widehat{\mathbf{Y}}_{\mathcal{V}_L} = \mathbf{Y}_{\mathcal{V}_L}$, which means that the GNN g perfectly estimates the observed labels. Therefore, the QW loss provides a new alternative for the training loss of GNN. Different from the traditional loss function in (2), the QW loss treats observed node labels and their estimations as two sets and measures their discrepancy accordingly, which provides an effective implementation of the loss in (3).

Applying the QW loss to learn a GNN g results in the following constrained optimization problem:

$$\min_{\theta} QW(g_{\mathcal{V}_L}(\mathbf{X}, \mathbf{A}; \theta), \mathbf{Y}_{\mathcal{V}_L}) = \min_{\theta} \min_{\mathbf{F} \in \Omega_C(\mathbf{S}_{\mathcal{V}_L}, g_{\mathcal{V}_L}(\mathbf{X}, \mathbf{A}; \theta), \mathbf{Y}_{\mathcal{V}_L})} \|\text{diag}(\mathbf{w}) \mathbf{F}\|_1. \quad (11)$$

To solve it effectively, we consider the following two algorithms.

3.3.1 Bregman Divergence-based Approximate Solver

By relaxing the constraint $\{\mathbf{F} | \mathbf{S}_{\mathcal{V}_L} \mathbf{F} = \mathbf{Y}_{\mathcal{V}_L} - g_{\mathcal{V}_L}(\mathbf{X}, \mathbf{A}; \theta)\}$ to a Bregman divergence-based regularizer (Benamou et al. 2015), we can reformulate (11) to the following problem:

$$\min_{\theta, \mathbf{F} \in \mathcal{U}^{|\mathcal{E}| \times C}} \|\text{diag}(\mathbf{w}) \mathbf{F}\|_1 + \lambda \underbrace{B_{\phi}(g_{\mathcal{V}_L}(\mathbf{X}, \mathbf{A}; \theta) + \mathbf{S}_{\mathcal{V}_L} \mathbf{F}, \mathbf{Y}_{\mathcal{V}_L})}_{\sum_{v \in \mathcal{V}_L} \psi(g_v(\mathbf{X}, \mathbf{A}; \theta) + \mathbf{S}_v \mathbf{F}, \mathbf{y}_v)}. \quad (12)$$

Here, $B_{\phi}(x, y) = \phi(x) - \phi(y) - \langle \nabla \phi(y), x - y \rangle$ is the Bregman divergence defined based on the strictly convex function ϕ , and the hyperparameter $\lambda > 0$ controls its significance. In node classification tasks, we can set ϕ as an entropic function, and the Bregman divergence becomes the KL-divergence.

Algorithm 1 Learning a GNN by solving (12)

Require: A graph’s adjacency matrix \mathbf{A} , node features \mathbf{X} , and labels $\mathbf{Y}_{\mathcal{V}_L}$.

- 1: Initialize $\theta^{(0)}$ and $\mathbf{F}^{(0)}$ randomly.
 - 2: **while** Not converge **do**
 - 3: Compute Loss = $\|\text{diag}(\mathbf{w})\mathbf{F}\|_1 + \lambda B_\phi(g_{\mathcal{V}_L}(\mathbf{X}, \mathbf{A}; \theta) + \mathbf{S}_{\mathcal{V}_L}\mathbf{F}, \mathbf{Y}_{\mathcal{V}_L})$.
 - 4: Update $\{\mathbf{F}, \theta\}$ by Adam (Kingma and Ba 2014).
 - 5: **if** G is a directed graph **then** $\mathbf{F} \leftarrow \text{Proj}_{\geq 0}(\mathbf{F})$ **end if**.
 - 6: **return** Optimal label transport \mathbf{F}^* and model parameters θ^* .
-

Algorithm 2 Learning a GNN by solving (13)

Require: A graph G , its adjacency matrix \mathbf{A} (edge weights \mathbf{w}), node features \mathbf{X} , observed labels $\mathbf{Y}_{\mathcal{V}_L}$, the number of inner iterations J .

- 1: Initialize $\theta^{(0)}$ and $\mathbf{F}^{(0)}$ randomly and set $\mathbf{Z}^{(0)} = \mathbf{0}_{|\mathcal{V}_L| \times C}$.
 - 2: **while** Not converge **do**
 - 3: Solve (14) by Adam (Kingma and Ba 2014) with J steps and obtain $\theta^{(k+1)}$.
 - 4: Solve (15) by Adam (Kingma and Ba 2014) with J steps and obtain $\mathbf{F}^{(k+1)}$.
 - 5: **if** G is a directed graph **then** $\mathbf{F}^{(k+1)} \leftarrow \text{Proj}_{\geq 0}(\mathbf{F}^{(k+1)})$ **end if**.
 - 6: Obtain $\mathbf{Z}^{(k+1)}$ by (16).
 - 7: **return** Optimal label transport \mathbf{F}^* and model parameters θ^* .
-

In node regression tasks, we can set ϕ as a least-square loss, and the Bregman divergence becomes the least-square loss. Therefore, as shown in (12), the Bregman divergence B_ϕ can be implemented based on commonly-used loss functions, e.g., the ψ in (2).

Algorithm 1 shows the algorithmic scheme in details. For undirected graphs, the \mathcal{U} in (12) is \mathbb{R} , and accordingly, (12) becomes a unconstrained optimization problem. We can solve it efficiently by gradient descent. For directed graphs, we just need to add a projection step when updating the flow matrix \mathbf{F} , leading to the projected gradient descent algorithm.

3.3.2 Bregman ADMM-based Exact Solver

Algorithm 1 solves (11) approximately — because of relaxing the strict equality constraint to a regularizer, the solution of (12) often cannot satisfy the original equality constraint. To solve (11) exactly, we further develop a learning method based on the Bregman ADMM (Bregman Alternating Direction Method of Multipliers) algorithm (Wang and Banerjee 2014). In particular, we can rewrite (11) in the following augmented Lagrangian form:

$$\begin{aligned} \min_{\theta, \mathbf{F} \in \mathcal{U}^{|\mathcal{E}| \times C}, \mathbf{Z} \in \mathbb{R}^{|\mathcal{V}_L| \times C}} & \|\text{diag}(\mathbf{w})\mathbf{F}\|_1 \\ & + \langle \mathbf{Z}, g_{\mathcal{V}_L}(\mathbf{X}, \mathbf{A}; \theta) + \mathbf{S}_{\mathcal{V}_L}\mathbf{F} - \mathbf{Y}_{\mathcal{V}_L} \rangle + \lambda B_\phi(g_{\mathcal{V}_L}(\mathbf{X}, \mathbf{A}; \theta) + \mathbf{S}_{\mathcal{V}_L}\mathbf{F}, \mathbf{Y}_{\mathcal{V}_L}), \end{aligned} \quad (13)$$

where $\mathbf{Z} \in \mathbb{R}^{|\mathcal{V}_L| \times C}$ is the dual variable, the second term in (13) is the Lagrangian term corresponding to the equality constraint, and the third term in (13) is the augmented term implemented as the Bregman divergence.

Denote the objective function in (13) as $L(\theta, \mathbf{F}, \mathbf{Z})$. In the Bregman ADMM framework, we can optimize θ , \mathbf{F} , and \mathbf{Z} iteratively through alternating optimization. In the k -th iteration, we update the three variables via solving the following three subproblems:

$$\begin{aligned} \theta^{(k+1)} &= \arg \min_{\theta} L(\theta, \mathbf{F}^{(k)}, \mathbf{Z}^{(k)}) \\ &= \arg \min_{\theta} \langle \mathbf{Z}^{(k)}, g_{\mathcal{V}_L}(\mathbf{X}, \mathbf{A}; \theta) \rangle + \lambda B_\phi(g_{\mathcal{V}_L}(\mathbf{X}, \mathbf{A}; \theta) + \mathbf{S}_{\mathcal{V}_L}\mathbf{F}^{(k)}, \mathbf{Y}_{\mathcal{V}_L}). \end{aligned} \quad (14)$$

Table 1: Comparison between traditional methods and ours.

Method	Setting	Node Classification	Node Regression
Apply the loss in (2)	ψ	Cross-entropy or KL	Least-square
	Predicted \mathbf{y}_v	$g_v(\mathbf{X}, \mathbf{A}; \theta), \forall v \in \mathcal{V} \setminus \mathcal{V}_L$	
Apply the QW loss	ϕ	Entropy	$\frac{1}{2} \ \cdot\ _2^2$
	$B_\phi (= \psi)$	KL	Least-square
	Predicted \mathbf{y}_v	$g_v(\mathbf{X}, \mathbf{A}; \theta) + \mathbf{S}_v \mathbf{F}, \forall v \in \mathcal{V} \setminus \mathcal{V}_L$	

$$\begin{aligned}
 \mathbf{F}^{(k+1)} &= \arg \min_{\mathbf{F} \in \mathcal{U}^{|\mathcal{E}| \times C}} L(\theta^{(k+1)}, \mathbf{F}, \mathbf{Z}^{(k)}) \\
 &= \arg \min_{\mathbf{F} \in \mathcal{U}^{|\mathcal{E}| \times C}} \|\text{diag}(\mathbf{w}) \mathbf{F}\|_1 + \langle \mathbf{Z}^{(k)}, \mathbf{S}_{\mathcal{V}_L} \mathbf{F} \rangle \\
 &\quad + \lambda B_\phi(g_{\mathcal{V}_L}(\mathbf{X}, \mathbf{A}; \theta^{(k+1)}) + \mathbf{S}_{\mathcal{V}_L} \mathbf{F}, \mathbf{Y}_{\mathcal{V}_L}).
 \end{aligned} \tag{15}$$

$$\mathbf{Z}^{(k+1)} = \mathbf{Z}^{(k)} + \lambda(g_{\mathcal{V}_L}(\mathbf{X}, \mathbf{A}; \theta^{(k+1)}) + \mathbf{S}_{\mathcal{V}_L} \mathbf{F}^{(k+1)} - \mathbf{Y}_{\mathcal{V}_L}). \tag{16}$$

We can find that (14) is a unconstrained optimization problem, so we can update the model parameter θ by gradient descent. Similarly, we can solve (15) and update the flow matrix \mathbf{F} by gradient descent or projected gradient descent, depending on whether the graph is undirected or not. Finally, the update of the dual variable \mathbf{Z} can be achieved in a closed form, as shown in (16). The Bregman ADMM algorithm solves the original problem in (12) rather than a relaxed version. In theory, with the increase of iterations, we can obtain the optimal variables that satisfy the equality constraint. Algorithm 2 shows the scheme of the Bregman ADMM-based solver.

3.3.3 Optional Edge Weight Prediction

Some GNNs, e.g., GCN-LPA (Wang and Leskovec 2021) and GAT (Veličković et al. 2018), model the adjacency matrix of graph as learnable parameters. Inspired by these models, we can optionally introduce an edge weight predictor and parameterize the adjacency matrix based on the flow matrix, as shown in Figure 1. In particular, given \mathbf{F} , we can apply a multi-layer perceptron (MLP) to embed it to an edge weight vector and then obtain a weighted adjacency matrix. Accordingly, the learning problem becomes

$$\min_{\theta, \xi} \min_{\mathbf{F} \in \Omega_C(\mathbf{S}_{\mathcal{V}_L}; g_{\mathcal{V}_L}(\mathbf{X}, \mathbf{A}(\mathbf{F}; \xi); \theta), \mathbf{Y}_{\mathcal{V}_L})} \|\text{diag}(\mathbf{w}) \mathbf{F}\|_1, \tag{17}$$

where $\mathbf{A}(\mathbf{F}; \xi)$ represents the adjacency matrix determined by the label transportation \mathbf{F} , and ξ represents the parameters of the MLP. Taking the learning of ξ into account, we can modify the above two solvers slightly and make them applicable for solving (17).

3.4 Connections to Traditional Methods

As discussed in Section 3.3.1 and shown in (12), the Bregman divergence B_ϕ can be implemented as the commonly-used loss function ψ in (2) (e.g., the KL divergence or the least-square loss). Table 1 compares the typical setting of traditional learning methods and that of our QW loss-based method in different node-level tasks. Essentially, the traditional learning method in (2) can be viewed as a special case of our QW loss-based learning method. In particular, when setting $\mathbf{F} = \mathbf{0}_{|\mathcal{E}| \times C}$ and $B_\phi = \psi$, the objective function in (12) degrades to the objective function in (2), which treats each node independently. Similarly, when further setting the dual variable $\mathbf{Z} = \mathbf{0}_{|\mathcal{V}_L| \times C}$, the objective function in (13) degrades to the objective function in (2) as well. In theory, we demonstrate that

our QW loss-based learning method can fit training data better than the traditional method does, as shown in the following theorem.

Theorem 3. *Let $\{\theta^*, \mathbf{F}^*, \mathbf{Z}^*\}$ be the global optimal solution of (13), $\{\theta^\dagger, \mathbf{F}^\dagger\}$ be the global optimal solution of (12), and θ^\ddagger be the global optimal solution of $\min_{\theta} B_{\phi}(g_{\mathcal{V}_L}(\mathbf{X}, \mathbf{A}; \theta), \mathbf{Y}_{\mathcal{V}_L})$, we have*

$$B_{\phi}(g_{\mathcal{V}_L}(\mathbf{X}, \mathbf{A}; \theta^*) + \mathbf{S}_{\mathcal{V}_L} \mathbf{F}^*, \mathbf{Y}_{\mathcal{V}_L}) \leq B_{\phi}(g_{\mathcal{V}_L}(\mathbf{X}, \mathbf{A}; \theta^\dagger) + \mathbf{S}_{\mathcal{V}_L} \mathbf{F}^\dagger, \mathbf{Y}_{\mathcal{V}_L}) \leq B_{\phi}(g_{\mathcal{V}_L}(\mathbf{X}, \mathbf{A}; \theta^\ddagger), \mathbf{Y}_{\mathcal{V}_L})$$

Proof. The proof is straightforward — $\{\theta^\ddagger, \mathbf{0}_{|\mathcal{E}| \times C}\}$ is a feasible solution of (12), so the corresponding objective is equal to or larger than that obtained by $\{\theta^\dagger, \mathbf{F}^\dagger\}$. Similarly, $\{\theta^\dagger, \mathbf{F}^\dagger, \mathbf{0}_{|\mathcal{V}_L| \times C}\}$ is a feasible solution of (13), so the corresponding objective is equal to or larger than that obtained by $\{\theta^*, \mathbf{F}^*, \mathbf{Z}^*\}$. \square

Remark. Although the Bregman ADMM-based solver can fit training data better in theory, in the cases with distribution shifting or out-of-distribution issues, it has a higher risk of overfitting. Therefore, in practice, we can select one of the above two solvers to optimize the GW loss, depending on their performance. In the following experiments, we will compare these two solvers in details.

3.5 A New Transductive Prediction Paradigm

As shown in Table 1, given the learned model θ^* and the optimal label transport \mathbf{F}^* , we predict node labels in a new transductive prediction paradigm. For $v \in \mathcal{V} \setminus \mathcal{V}_L$, we predict its label as

$$\tilde{\mathbf{y}}_v := g_v(\mathbf{X}, \mathbf{A}; \theta^*) + \mathbf{S}_v \mathbf{F}^*, \tag{18}$$

which combines the estimated label from the learned GNN and the residual component from the optimal label transport.

It should be noted that some attempts have been made to incorporate label propagation algorithms (LPAs) (Zhu and Goldberg 2022) into GNNs, e.g., the GCN-LPA in (Wang and Leskovec 2021) and the FDiff-Scale in (Huang et al. 2021). The PTA in (Dong et al. 2021) demonstrates that learning a decoupled GNN is equivalent to implementing a label propagation algorithm. These methods leverage LPAs to regularize the learning of GNNs. However, in the prediction phase, they abandon the training labels and rely only on the GNNs to predict node labels, as shown in Table 1. Unlike these methods, our QW loss-based method achieves a new OT-based label propagation mechanism, saving the training label information in the optimal label transport and applying it explicitly in the prediction phase.

4 Experiments

To demonstrate the effectiveness of our QW loss-based learning method, we apply it to learn GNNs with various architectures and test the learned GNNs in different node-level prediction tasks. We compare our learning method with the traditional one in (2) on their model performance and computational efficiency. For our method, we conduct a series of analytic experiments to show its robustness to hyperparameter settings and label insufficiency. All the experiments are conducted on a machine with three NVIDIA A40 GPUs, and the code is implemented based on PyTorch.

Table 2: Basic information of the graphs and the comparisons on node classification accuracy (%).

Model	Method	Homophilic graphs					Heterophilic graphs					Overall Improve
		Cora	Citeseer	Pubmed	Computers	Photo	Squirrel	Chameleon	Actor	Texas	Cornell	
		2708	3,327	19,717	13,752	7650	5,201	2,277	7,600	183	183	
		1,433	3,703	500	767	745	2,089	2,325	932	1,703	1,703	
		5,278	4,552	44,324	245,861	119,081	198,423	31,371	26,659	279	277	
		81.0%	73.6%	80.2%	77.7%	82.7%	22.2%	23.0%	21.8%	6.1%	12.3%	
		7	6	3	10	8	5	5	5	5	5	
GCN	(2)	87.44±0.96	79.98±0.84	86.93±0.29	88.42±0.45	93.24±0.43	46.55±1.15	63.57±1.16	34.00±1.28	77.21±3.28	61.91±5.11	—
	(2)+LPA	86.34±1.45	78.51±1.22	84.72±0.70	82.48±0.69	88.10±1.31	44.81±1.81	60.90±1.63	32.43±1.59	78.69±6.47	68.72±5.95	-1.36
GAT	QW	87.88±0.79	81.36±0.41	87.89±0.40	89.20±0.41	93.81±0.36	52.62±0.49	68.10±1.01	38.09±0.50	84.10±2.95	84.26±2.98	+4.81
	(2)	89.20±0.79	80.75±0.78	87.42±0.33	90.08±0.36	94.38±0.25	48.20±1.67	64.31±2.01	35.68±0.60	80.00±3.11	68.09±2.13	—
GIN	QW	89.11±0.66	80.19±0.64	88.38±0.23	90.41±0.28	94.65±0.24	55.03±1.35	67.35±1.42	33.86±2.13	80.33±1.80	70.21±2.13	+1.14
	(2)	86.22±0.95	76.18±0.78	87.87±0.23	80.87±1.43	89.83±0.72	39.11±2.23	64.29±1.51	32.37±1.56	72.79±4.92	62.55±4.80	—
GraphSAGE	QW	86.24±0.90	76.13±1.09	87.53±0.34	89.28±0.45	92.60±0.44	65.29±0.68	73.26±1.12	32.32±1.93	77.54±2.60	64.04±3.62	+5.22
	(2)	88.24±0.95	79.81±0.80	88.14±0.25	89.71±0.38	95.08±0.26	43.79±0.59	63.26±1.09	38.99±0.85	90.00±2.30	84.26±2.98	—
APPNP	QW	87.59±0.77	80.52±0.68	88.61±0.32	90.17±0.24	95.25±0.25	54.37±0.89	68.32±0.68	37.82±0.45	90.33±1.97	86.38±2.13	+1.18
	(2)	88.33±0.77	81.28±0.71	88.62±0.33	86.27±0.37	93.70±0.27	36.15±0.75	52.93±1.71	40.46±0.64	91.31±1.97	87.66±2.13	—
BernNet	QW	88.74±0.84	80.94±0.61	89.48±0.28	86.95±0.82	94.43±0.24	38.73±1.06	53.76±1.25	40.78±0.74	91.48±2.30	87.87±2.34	+0.65
	(2)	88.28±1.00	79.81±0.79	88.87±0.38	87.61±0.46	93.68±0.28	51.15±1.09	67.96±1.05	40.72±0.80	93.28±1.48	90.21±2.35	—
ChebNetII	QW	89.03±0.76	81.35±0.71	89.03±0.38	89.58±0.47	94.55±0.39	55.22±0.64	71.66±1.18	40.91±0.71	93.44±1.80	90.85±2.34	+1.41
	(2)	88.26±0.89	80.00±0.74	88.57±0.36	86.58±0.71	93.50±0.34	57.78±0.84	71.71±1.40	40.70±0.77	92.79±1.48	88.94±2.78	—
	QW	88.54±0.76	79.47±0.70	89.47±0.36	90.43±0.22	94.84±0.37	60.55±0.64	74.05±0.68	41.37±0.67	93.93±0.98	87.23±3.62	+1.11

4.1 Implementation Details

4.1.1 Datasets

The datasets we considered consist of five homophilic graphs (i.e., **Cora**, **Citeseer**, **Pubmed** (Sen et al. 2008, Yang et al. 2016), **Computers**, and **Photo** (McAuley et al. 2015)) and five heterophilic graphs (i.e., **Chameleon**, **Squirrel** (Rozemberczki et al. 2021), **Actor**, **Texas**, and **Cornell** (Pei et al. 2020)), respectively. Following the work in (Wang and Leskovec 2021), we categorize the graphs according to the percentage of the edges connecting the nodes of the same class (i.e., the intra-edge rate). The basic information of these graphs is shown in Table 2. Additionally, a large **arXiv-year** graph (Lim et al. 2021) is applied to demonstrate the efficiency of our method. The adjacency matrix of each graph is binary, so the edge weights $\mathbf{w} = \mathbf{1}_{|\mathcal{E}|}$.

4.1.2 GNN Architectures

In the following experiments, the models we considered include *i*) the representative spatial GNNs, i.e., **GCN** (Kipf and Welling 2017), **GAT** (Veličković et al. 2018), **GIN** (Xu et al. 2019a), **GraphSAGE** (Hamilton et al. 2017), and **GCN-LPA** (Wang and Leskovec 2021) that combines the GCN with the label propagation algorithm; and *ii*) state-of-the-art spectral GNNs, i.e., **APPNP** (Gasteiger et al. 2019), **BernNet** (He et al. 2021), and **ChebNetII** (He et al. 2022). For a fair comparison, we set the architectures of the GNNs based on the code provided by (He et al. 2022) and configure the algorithmic hyperparameters by grid search. More details of the hyperparameter settings are in Appendix.

4.1.3 Learning Tasks and Evaluation Measurements

For each graph, their nodes belong to different classes. Therefore, we first learn different GNNs to solve the node-level classification tasks defined on the above graphs. By default, the split ratio of each graph’s nodes is 60% for training, 20% for validation, and 20% for testing, respectively. The GNNs are learned by *i*) the traditional learning method in (2)¹ and *ii*) minimizing the proposed

¹For GCN-LPA (Wang and Leskovec 2021), it learns a GCN model by imposing a label propagation-based regularizer on (2) and adjusting edge weights by the propagation result.

Table 3: Comparisons on node regression error (MSE).

Model	Method	Homophilic graphs		Heterophilic graphs	
		Computers	Photo	Actor	Cornell
GIN	(2)	0.0605 \pm 0.0018	0.0459 \pm 0.0044	0.1570 \pm 0.0014	0.1609 \pm 0.0359
	QW	0.0244\pm0.0028	0.0203\pm0.0012	0.1564\pm0.0012	0.1524\pm0.0043
BernNet	(2)	0.0871 \pm 0.0002	0.0488 \pm 0.0009	0.1661\pm0.0020	0.0989 \pm 0.0076
	QW	0.0364\pm0.0038	0.0297\pm0.0014	0.1671 \pm 0.0008	0.0753\pm0.0024

QW loss in (11), respectively. When implementing the QW loss, we apply either Algorithm 1 or 2, depending on their performance. Additionally, to demonstrate the usefulness of our QW loss in node-level regression tasks, we treat the node labels as one-hot vectors and fit them by minimizing the mean squared error (MSE), in which the ψ in (2) and the corresponding Bregman divergence B_ϕ are set to be the least-square loss. For each method, we perform 10 runs with different seeds and record the learning results’ mean and standard deviation.

4.2 Numerical Comparison and Visualization

4.2.1 Node Classification and Regression

Table 2 shows the node classification results on the ten graphs,² whose last column records the overall improvements caused by our QW loss compared to other learning methods. The experimental results demonstrate the usefulness of our QW loss-based learning method — for each model, applying our QW loss helps to improve learning results in most situations and leads to consistent overall improvements. In particular, for the state-of-the-art spectral GNNs like BernNet (He et al. 2021) and ChebNetII (He et al. 2022), learning with our QW loss can improve their overall performance on both homophilic and heterophilic graphs consistently, resulting in the best performance in this experiment. For the simple GCN model (Kipf and Welling 2017), learning with our QW loss improves its performance significantly and reduces the gap between its classification accuracy and that of the state-of-the-art models (Gasteiger et al. 2019, He et al. 2021, 2022), especially heterophilic graphs. Note that, when learning GCN, our QW loss works better than the traditional method regularized by the label propagation (i.e., GCN-LPA (Wang and Leskovec 2021)) because our learning method can leverage the training label information in both learning and prediction phases. GCN-LPA improves GCN when learning on heterophilic graphs, but surprisingly, leads to performance degradation on homophilic graphs. Additionally, we also fit the one-hot labels by minimizing the MSE. As shown in Table 3, minimizing the QW loss leads to lower MSE results, which demonstrates the usefulness of the QW loss in node-level regression tasks.

4.2.2 Computational Efficiency and Scalability

In theory, the computational complexity of our QW loss is linear with the number of edges. When implementing the loss as (13) and solving it by Algorithm 2, its complexity is also linear with the number of inner iterations J . Figure 2 shows the runtime comparisons for the QW loss-based learning methods and the traditional method on two datasets. We can find that minimizing the QW loss by Algorithm 1 or Algorithm 2 with $J = 1$ merely increases the training time slightly compared to the traditional method. Empirically, setting $J \leq 5$ can lead to promising learning results, as shown in Tables 2 and 3. In other words, the computational cost of applying the QW

²In Table 2, we bold the best learning result for each graph. Learning GCN by “(2)+LPA” means implementing GCN-LPA (Wang and Leskovec 2021).

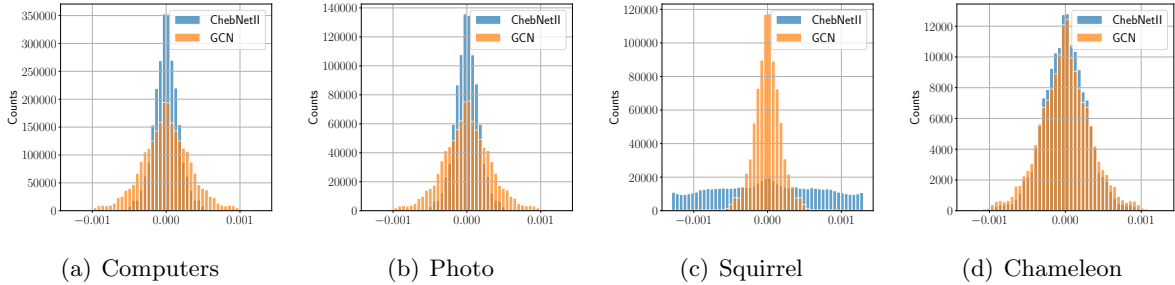


Figure 3: The histogram of \mathbf{F}^* 's values for different GNNs.

loss is tolerable considering the significant performance improvements it achieved. Additionally, we apply our QW loss to large-scale graphs and test its scalability. As shown in Table 4, we implement the QW loss based on Algorithm 1 (i.e., solving (12)) and apply it to the node classification task in the large-scale arXiv-year graph. The result shows that our QW loss is applicable to the graphs with millions of edges on a single GPU and improves the model performance.

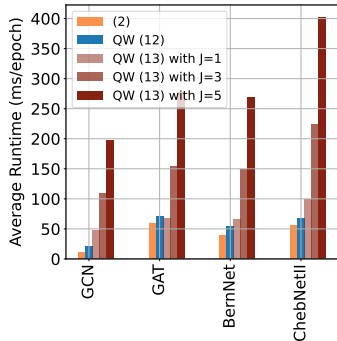


Figure 2: The runtime of different learning methods on the Photo graph.

Graph	arXiv-year
#Nodes ($ \mathcal{V} $)	169,343
#Features (D)	128
#Edges ($ \mathcal{E} $)	1,166,243
Intra-edge rate	22.0%
#Classes (C)	5
ChebNetII (2)	48.18 ± 0.18
QW	48.30 ± 0.25

Table 4: The node classification accuracy (%) on a large graph.

4.2.3 Distribution of Optimal Label Transport

Figure 3 visualizes the histograms of the optimal label transport \mathbf{F}^* learned for two representative GNNs (i.e., GCN (Kipf and Welling 2017) and ChebNetII (He et al. 2022)) on four graphs (i.e., the homophilic graphs “Computers” and “Photo” and the heterophilic graphs “Squirrel” and “Chameleon”). We can find that when learning on homophilic graphs, the elements of the optimal label transport obey the zero-mean Laplacian distribution. It is reasonable from the perspective of optimization — the term $\|\text{diag}(\mathbf{w})\mathbf{F}\|_1$ can be explained as a Laplacian prior imposed on \mathbf{F} 's element. Additionally, we can find that the distribution corresponding to GCN has larger variance than that corresponding to ChebNetII, which implies that the \mathbf{F}^* of GCN has more non-zero elements and thus has more significant impacts on label prediction. The numerical results in Table 2 can also verify this claim — in most situations, the performance improvements caused by the optimal label transport is significant for GCN but slight for ChebNetII. For heterophilic graphs, learning GCN still leads to Laplacian distributed label transport. However, the distributions corresponding to ChebNetII are diverse — the distribution for Squirrel is long-tailed while that for Chameleon is still Laplacian.

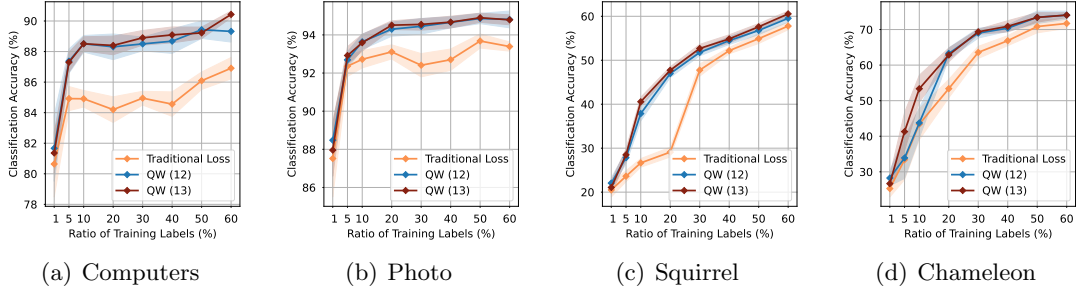


Figure 4: Illustrations of the learning methods’ performance given different amounts of labeled nodes.

Table 5: Impacts of adjusting edge weights on node classification accuracy (%) when applying the QW loss.

Model		Homophilic		Heterophilic	
		Computers	Photo	Actor	Cornell
GCN	\mathbf{A}	88.39 \pm 0.55	93.80 \pm 0.37	30.14 \pm 0.80	60.64 \pm 4.26
	$\mathbf{A}(\mathbf{F}; \xi)$	84.35 \pm 0.46	91.79 \pm 0.21	38.09 \pm 0.50	84.26 \pm 2.98
ChebNetII	\mathbf{A}	89.52 \pm 0.54	94.84 \pm 0.37	41.37 \pm 0.67	86.38 \pm 3.19
	$\mathbf{A}(\mathbf{F}; \xi)$	89.41 \pm 0.41	94.79 \pm 0.45	40.74 \pm 0.80	86.60 \pm 2.98

4.3 Analytic Experiments

4.3.1 Robustness to Label Insufficiency Issue

Our QW loss-based learning method considers the label transport on graphs, whose feasible domain is determined by the observed training labels. The more labels we observed, the smaller the feasible domain is. To demonstrate the robustness of our method to the label insufficiency issue, we evaluate the performance of our method given different amounts of training labels. We train ChebNetII (He et al. 2022) on four graphs by traditional method and our method, respectively. For each graph, we use $K\%$ nodes’ labels to train the ChebNetII, where $K \in [1, 60]$, and apply 20% nodes for testing. Figure 4 shows that our QW loss-based learning method can achieve encouraging performance even when only 20% nodes or fewer are labeled. Additionally, the methods are robust to the selection of solver.

4.3.2 Impacts of Adjusting Edge Weights

As shown in (17), we can train an MLP to predict edge weights based on the optimal label transport. The ablation study in Table 5 quantitatively show the impacts of adjusting edge weights on the learning results. We can find that for ChebNetII, the two settings provide us with comparable learning results. For GCN, however, learning the model with adjusted edge weights suffers from performance degradation on homophilic graphs while leads to significant improvements on heterophilic graphs. Empirically, it seems that adjusting edge weights based on label transportation helps to improve the learning of simple GNN models on heterophilic graphs.

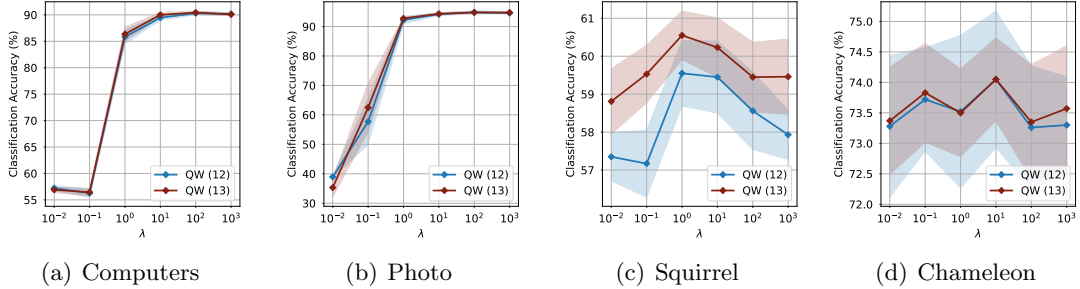


Figure 5: The impact of λ on the learning results.

4.3.3 Robustness to Hyperparameters

The weight of the Bregman divergence term, i.e., λ , is the key hyperparameter impacting the performance of our learning method. Empirically, when λ is too small, the Bregman divergence between the observed labels and their predictions becomes ignorable. Accordingly, the regularizer may be too weak to supervise GNNs’ learning properly. On the contrary, when λ is too large, the regularizer becomes dominant in the learning objective, and the impact of the label transport becomes weak in both the learning and prediction phases. As a result, it may perform similarly to the traditional method when using a large λ . We test the robustness of our method to λ and show representative results in Figure 5. In particular, our QW loss-based method trains ChebNetII (He et al. 2022) on four graphs. Both Algorithm 1 for (12) and Algorithm 2 for (13) are tested. The λ is set in the range from 10^{-2} to 10^3 . For homophilic graphs, our learning method achieves stable performance when $\lambda \geq 10$. When $\lambda < 10$, the learning results degrade significantly because of inadequate supervision. Our learning method often obtains the best learning result for heterophilic graphs when $\lambda \in [1, 10]$. These results show that our method is robust to λ , and we can set λ in a wide range to obtain relatively stable performance.

5 Conclusion

We have proposed the Quasi-Wasserstein loss for learning graph neural networks. This loss matches well with the non-i.i.d. property of graph-structured data, providing a new strategy to leverage observed node labels in both training and testing phases. Applying the QW loss to learn GNNs improves their performance in various node-level prediction tasks. In the future, we would like to explore the impacts of the optimal label transport on the generalization power of GNNs in theory. Moreover, we plan to modify the QW loss further, developing a new optimization strategy to accelerate its computation.

Acknowledgements

This work was supported by the National Natural Science Foundation of China (No. 92270110, No. 62106271), CAAI-Huawei MindSpore Open Fund, the Fundamental Research Funds for the Central Universities, and the Research Funds of Renmin University of China. Hongteng Xu also would like to thank the supports from the Beijing Key Laboratory of Big Data Management and Analysis Methods, the Intelligent Social Governance Platform, Major Innovation & Planning Interdisciplinary Platform for the “Double-First Class” Initiative.

References

- Martin Arjovsky, Soumith Chintala, and Léon Bottou. 2017. Wasserstein generative adversarial networks. In *International conference on machine learning*. PMLR, 214–223.
- Muhammet Balcilar, Renton Guillaume, Pierre Héroux, Benoit Gaüzère, Sébastien Adam, and Paul Honeine. 2021. Analyzing the expressive power of graph neural networks in a spectral perspective. In *International Conference on Learning Representations*.
- Jean-David Benamou, Guillaume Carlier, Marco Cuturi, Luca Nenna, and Gabriel Peyré. 2015. Iterative Bregman projections for regularized transportation problems. *SIAM Journal on Scientific Computing* 37, 2 (2015), A1111–A1138.
- Filippo Maria Bianchi, Daniele Grattarola, Lorenzo Livi, and Cesare Alippi. 2021. Graph neural networks with convolutional arma filters. *IEEE transactions on pattern analysis and machine intelligence* 44, 7 (2021), 3496–3507.
- Benson Chen, Gary Bécigneul, Octavian-Eugen Ganea, Regina Barzilay, and Tommi Jaakkola. 2020. Optimal transport graph neural networks. *arXiv preprint arXiv:2006.04804* (2020).
- Eli Chien, Jianhao Peng, Pan Li, and Olgica Milenkovic. 2021. Adaptive Universal Generalized PageRank Graph Neural Network. In *International Conference on Learning Representations*.
- Marco Cuturi. 2013. Sinkhorn distances: lightspeed computation of optimal transport. In *Proceedings of the 26th International Conference on Neural Information Processing Systems-Volume 2*. 2292–2300.
- Michaël Defferrard, Xavier Bresson, and Pierre Vandergheynst. 2016. Convolutional neural networks on graphs with fast localized spectral filtering. In *Proceedings of the 30th International Conference on Neural Information Processing Systems*. 3844–3852.
- Hande Dong, Jiawei Chen, Fuli Feng, Xiangnan He, Shuxian Bi, Zhaolin Ding, and Peng Cui. 2021. On the equivalence of decoupled graph convolution network and label propagation. In *Proceedings of the Web Conference 2021*. 3651–3662.
- Yihe Dong and Will Sawin. 2020. Copt: Coordinated optimal transport on graphs. *Advances in Neural Information Processing Systems* 33 (2020), 19327–19338.
- Lun Du, Xiaozhou Shi, Qiang Fu, Xiaojun Ma, Hengyu Liu, Shi Han, and Dongmei Zhang. 2022. Gbk-gnn: Gated bi-kernel graph neural networks for modeling both homophily and heterophily. In *Proceedings of the ACM Web Conference 2022*. 1550–1558.
- Montacer Essid and Justin Solomon. 2018. Quadratically regularized optimal transport on graphs. *SIAM Journal on Scientific Computing* 40, 4 (2018), A1961–A1986.
- Enrico Facca and Michele Benzi. 2021. Fast iterative solution of the optimal transport problem on graphs. *SIAM Journal on Scientific Computing* 43, 3 (2021), A2295–A2319.
- Wenqi Fan, Yao Ma, Qing Li, Yuan He, Eric Zhao, Jiliang Tang, and Dawei Yin. 2019. Graph neural networks for social recommendation. In *The world wide web conference*. 417–426.
- Charlie Frogner, Chiyuan Zhang, Hossein Mobahi, Mauricio Araya-Polo, and Tomaso Poggio. 2015. Learning with a Wasserstein loss. In *Proceedings of the 28th International Conference on Neural Information Processing Systems-Volume 2*. 2053–2061.

- Xinyu Fu, Jiani Zhang, Ziqiao Meng, and Irwin King. 2020. Magnn: Metapath aggregated graph neural network for heterogeneous graph embedding. In *Proceedings of The Web Conference 2020*. 2331–2341.
- Johannes Gasteiger, Aleksandar Bojchevski, and Stephan Günnemann. 2019. Predict then Propagate: Graph Neural Networks meet Personalized PageRank. In *International Conference on Learning Representations*.
- Edouard Grave, Armand Joulin, and Quentin Berthet. 2019. Unsupervised alignment of embeddings with wasserstein procrustes. In *The 22nd International Conference on Artificial Intelligence and Statistics*. PMLR, 1880–1890.
- Jingwei Guo, Kaizhu Huang, Xinpeng Yi, and Rui Zhang. 2023. Graph Neural Networks with Diverse Spectral Filtering. In *Proceedings of the ACM Web Conference 2023*. 306–316.
- William L Hamilton, Rex Ying, and Jure Leskovec. 2017. Inductive representation learning on large graphs. In *Proceedings of the 31st International Conference on Neural Information Processing Systems*. 1025–1035.
- Mingguo He, Zhewei Wei, and Ji-Rong Wen. 2022. Convolutional neural networks on graphs with chebyshev approximation, revisited. *Advances in Neural Information Processing Systems* 35 (2022), 7264–7276.
- Mingguo He, Zhewei Wei, Hongteng Xu, et al. 2021. Bernnet: Learning arbitrary graph spectral filters via bernstein approximation. *Advances in Neural Information Processing Systems* 34 (2021), 14239–14251.
- Qian Huang, Horace He, Abhay Singh, Ser-Nam Lim, and Austin Benson. 2021. Combining Label Propagation and Simple Models out-performs Graph Neural Networks. In *International Conference on Learning Representations*.
- Dejun Jiang, Zhenxing Wu, Chang-Yu Hsieh, Guangyong Chen, Ben Liao, Zhe Wang, Chao Shen, Dongsheng Cao, Jian Wu, and Tingjun Hou. 2021. Could graph neural networks learn better molecular representation for drug discovery? A comparison study of descriptor-based and graph-based models. *Journal of cheminformatics* 13, 1 (2021), 1–23.
- Diederik P Kingma and Jimmy Ba. 2014. Adam: A method for stochastic optimization. *arXiv preprint arXiv:1412.6980* (2014).
- Thomas N Kipf and Max Welling. 2017. Semi-Supervised Classification with Graph Convolutional Networks. In *International Conference on Learning Representations*.
- Johannes Klicpera, Stefan Weißenberger, and Stephan Günnemann. 2019. Diffusion improves graph learning. In *Proceedings of the 33rd International Conference on Neural Information Processing Systems*. 13366–13378.
- John Lee, Max Dabagia, Eva L Dyer, and Christopher J Rozell. 2019. Hierarchical optimal transport for multimodal distribution alignment. In *Proceedings of the 33rd International Conference on Neural Information Processing Systems*. 13475–13485.
- Mengzhang Li and Zhanxing Zhu. 2021. Spatial-temporal fusion graph neural networks for traffic flow forecasting. In *Proceedings of the AAAI conference on artificial intelligence*, Vol. 35. 4189–4196.

- Derek Lim, Felix Hohne, Xiuyu Li, Sijia Linda Huang, Vaishnavi Gupta, Omkar Bhalerao, and Ser Nam Lim. 2021. Large Scale Learning on Non-Homophilous Graphs: New Benchmarks and Strong Simple Methods. In *Advances in Neural Information Processing Systems*, M. Ranzato, A. Beygelzimer, Y. Dauphin, P.S. Liang, and J. Wortman Vaughan (Eds.), Vol. 34. Curran Associates, Inc., 20887–20902. https://proceedings.neurips.cc/paper_files/paper/2021/file/ae816a80e4c1c56caa2eb4e1819cbb2f-Paper.pdf
- Julian McAuley, Christopher Targett, Qinfeng Shi, and Anton Van Den Hengel. 2015. Image-based recommendations on styles and substitutes. In *Proceedings of the 38th international ACM SIGIR conference on research and development in information retrieval*. 43–52.
- Mathias Niepert, Mohamed Ahmed, and Konstantin Kutzkov. 2016. Learning convolutional neural networks for graphs. In *International conference on machine learning*. PMLR, 2014–2023.
- Hongbin Pei, Bingzhe Wei, Kevin Chen-Chuan Chang, Yu Lei, and Bo Yang. 2020. Geom-GCN: Geometric Graph Convolutional Networks. In *International Conference on Learning Representations*.
- Gabriel Peyré and Marco Cuturi. 2019. Computational Optimal Transport. *Foundations and Trends® in Machine Learning* 11, 5-6 (2019), 355–607.
- Jiezhong Qiu, Jian Tang, Hao Ma, Yuxiao Dong, Kuansan Wang, and Jie Tang. 2018. Deepinf: Social influence prediction with deep learning. In *Proceedings of the 24th ACM SIGKDD international conference on knowledge discovery & data mining*. 2110–2119.
- Meng Qu, Yoshua Bengio, and Jian Tang. 2019. Gmnn: Graph markov neural networks. In *International conference on machine learning*. PMLR, 5241–5250.
- Benedek Rozemberczki, Carl Allen, and Rik Sarkar. 2021. Multi-scale attributed node embedding. *Journal of Complex Networks* 9, 2 (2021), cnab014.
- Filippo Santambrogio. 2015. *Optimal Transport for Applied Mathematicians: Calculus of Variations, PDEs, and Modeling*. Vol. 87. Birkhäuser.
- Victor Garcia Satorras, Emiel Hooeboom, and Max Welling. 2021. E (n) equivariant graph neural networks. In *International conference on machine learning*. PMLR, 9323–9332.
- Prithviraj Sen, Galileo Namata, Mustafa Bilgic, Lise Getoor, Brian Galligher, and Tina Eliassi-Rad. 2008. Collective classification in network data. *AI magazine* 29, 3 (2008), 93–93.
- Vayer Titouan, Nicolas Courty, Romain Tavenard, and Rémi Flamary. 2019. Optimal transport for structured data with application on graphs. In *International Conference on Machine Learning*. PMLR, 6275–6284.
- Ilya Tolstikhin, Olivier Bousquet, Sylvain Gelly, and Bernhard Schoelkopf. 2018. Wasserstein Auto-Encoders. In *International Conference on Learning Representations*.
- Petar Veličković, Guillem Cucurull, Arantxa Casanova, Adriana Romero, Pietro Liò, and Yoshua Bengio. 2018. Graph Attention Networks. In *International Conference on Learning Representations*.
- Cédric Villani. 2008. *Optimal transport: old and new*. Vol. 338. Springer Science & Business Media.

- Cédric Vincent-Cuaz, Titouan Vayer, Rémi Flamary, Marco Corneli, and Nicolas Courty. 2021. Online graph dictionary learning. In *International Conference on Machine Learning*. PMLR, 10564–10574.
- Huahua Wang and Arindam Banerjee. 2014. Bregman alternating direction method of multipliers. In *Proceedings of the 27th International Conference on Neural Information Processing Systems-Volume 2*. 2816–2824.
- Hongwei Wang and Jure Leskovec. 2021. Combining graph convolutional neural networks and label propagation. *ACM Transactions on Information Systems (TOIS)* 40, 4 (2021), 1–27.
- Xiao Wang, Houye Ji, Chuan Shi, Bai Wang, Yanfang Ye, Peng Cui, and Philip S Yu. 2019. Heterogeneous graph attention network. In *The world wide web conference*. 2022–2032.
- Xiaoyang Wang, Yao Ma, Yiqi Wang, Wei Jin, Xin Wang, Jiliang Tang, Caiyan Jia, and Jian Yu. 2020. Traffic flow prediction via spatial temporal graph neural network. In *Proceedings of the web conference 2020*. 1082–1092.
- Yuyang Wang, Jianren Wang, Zhonglin Cao, and Amir Barati Farimani. 2022. Molecular contrastive learning of representations via graph neural networks. *Nature Machine Intelligence* 4, 3 (2022), 279–287.
- Yujia Xie, Xiangfeng Wang, Ruijia Wang, and Hongyuan Zha. 2020. A fast proximal point method for computing exact wasserstein distance. In *Uncertainty in artificial intelligence*. PMLR, 433–453.
- Bingbing Xu, Huawei Shen, Qi Cao, Keting Cen, and Xueqi Cheng. 2019c. Graph convolutional networks using heat kernel for semi-supervised learning. In *Proceedings of the 28th International Joint Conference on Artificial Intelligence*. 1928–1934.
- Hongteng Xu. 2020. Gromov-Wasserstein factorization models for graph clustering. In *Proceedings of the AAAI conference on artificial intelligence*, Vol. 34. 6478–6485.
- Hongteng Xu, Jiachang Liu, Dixin Luo, and Lawrence Carin. 2022. Representing graphs via Gromov-Wasserstein factorization. *IEEE Transactions on Pattern Analysis and Machine Intelligence* 45, 1 (2022), 999–1016.
- Hongteng Xu, Dixin Luo, Hongyuan Zha, and Lawrence Carin. 2019b. Gromov-wasserstein learning for graph matching and node embedding. In *International conference on machine learning*. PMLR, 6932–6941.
- Keyulu Xu, Weihua Hu, Jure Leskovec, and Stefanie Jegelka. 2019a. How Powerful are Graph Neural Networks?. In *International Conference on Learning Representations*.
- Zhilin Yang, William Cohen, and Ruslan Salakhudinov. 2016. Revisiting semi-supervised learning with graph embeddings. In *International conference on machine learning*. PMLR, 40–48.
- Zeyu Zhang, Jiamou Liu, Xianda Zheng, Yifei Wang, Pengqian Han, Yupan Wang, Kaiqi Zhao, and Zijian Zhang. 2023. RSGNN: A Model-agnostic Approach for Enhancing the Robustness of Signed Graph Neural Networks. In *Proceedings of the ACM Web Conference 2023*. 60–70.
- Meiqi Zhu, Xiao Wang, Chuan Shi, Houye Ji, and Peng Cui. 2021. Interpreting and unifying graph neural networks with an optimization framework. In *Proceedings of the Web Conference 2021*. 1215–1226.

Xiaojin Zhu and Andrew B Goldberg. 2022. *Introduction to Semi-Supervised Learning*. Springer Nature.

Chenyi Zhuang and Qiang Ma. 2018. Dual graph convolutional networks for graph-based semi-supervised classification. In *Proceedings of the 2018 world wide web conference*. 499–508.

A The Proofs of Theorems

A.1 Proof of Theorem 1

Proof. The proof includes four parts:

- **Feasibility.** For $\boldsymbol{\mu}, \boldsymbol{\gamma} \in \text{Range}(\mathcal{S}_{\mathcal{V}})$, we have

$$W_1(\boldsymbol{\mu}, \boldsymbol{\gamma}) = \min_{\mathbf{f} \in \Omega(\mathcal{S}_{\mathcal{V}}, \boldsymbol{\mu}, \boldsymbol{\gamma})} \|\text{diag}(\mathbf{w})\mathbf{f}\|_1. \quad (19)$$

Because $\boldsymbol{\mu}, \boldsymbol{\gamma} \in \text{Range}(\mathcal{S}_{\mathcal{V}})$, the feasible domain $\Omega(\mathcal{S}_{\mathcal{V}}, \boldsymbol{\mu}, \boldsymbol{\gamma})$ is always non-empty and (19) is always feasible.

- **Positivity.** Obviously, the objective in (19) is nonnegative, so that $W_1(\boldsymbol{\mu}, \boldsymbol{\gamma}) \geq 0$, $\forall \boldsymbol{\mu}, \boldsymbol{\gamma} \in \text{Range}(\mathcal{S}_{\mathcal{V}})$. Moreover, let

$$\mathbf{f}^* = \arg \min_{\mathbf{f} \in \Omega(\mathcal{S}_{\mathcal{V}}, \boldsymbol{\mu}, \boldsymbol{\gamma})} \|\text{diag}(\mathbf{w})\mathbf{f}\|_1.$$

$W_1(\boldsymbol{\mu}, \boldsymbol{\gamma}) = 0$ when $\mathbf{f}^* = \mathbf{0}_{|\mathcal{E}|}$, which means $\boldsymbol{\mu} = \boldsymbol{\gamma}$. Therefore, $\forall \boldsymbol{\mu}, \boldsymbol{\gamma} \in \text{Range}(\mathcal{S}_{\mathcal{V}})$, $W_1(\boldsymbol{\mu}, \boldsymbol{\gamma}) \geq 0$ and the equality holds iff $\boldsymbol{\mu} = \boldsymbol{\gamma}$.

- **Symmetry.** If \mathbf{f}^* is the optimal solution of $W_1(\boldsymbol{\mu}, \boldsymbol{\gamma})$, $-\mathbf{f}^*$ will be the optimal solution of $W_1(\boldsymbol{\gamma}, \boldsymbol{\mu})$. Because the edge weight vector is nonnegative, we have $\|\text{diag}(\mathbf{w})\mathbf{f}^*\|_1 = \|\text{diag}(\mathbf{w})\mathbf{f}^*\|_1$. As a result, $W_1(\boldsymbol{\mu}, \boldsymbol{\gamma}) = W_1(\boldsymbol{\gamma}, \boldsymbol{\mu})$.
- **Triangle Inequality.** For $\boldsymbol{\mu}, \boldsymbol{\gamma}, \boldsymbol{\zeta} \in \text{Range}(\mathcal{S}_{\mathcal{V}})$, let

$$\begin{aligned} W_1(\boldsymbol{\mu}, \boldsymbol{\gamma}) &= \min_{\mathbf{f}_1 \in \Omega(\mathcal{S}_{\mathcal{V}}, \boldsymbol{\mu}, \boldsymbol{\gamma})} \|\text{diag}(\mathbf{w})\mathbf{f}_1\|_1, \\ W_1(\boldsymbol{\gamma}, \boldsymbol{\zeta}) &= \min_{\mathbf{f}_2 \in \Omega(\mathcal{S}_{\mathcal{V}}, \boldsymbol{\gamma}, \boldsymbol{\zeta})} \|\text{diag}(\mathbf{w})\mathbf{f}_2\|_1. \end{aligned}$$

Then, we have

$$\begin{aligned} &W_1(\boldsymbol{\mu}, \boldsymbol{\gamma}) + W_1(\boldsymbol{\gamma}, \boldsymbol{\zeta}) \\ &= \min_{\mathbf{f}_1, \mathbf{f}_2} \|\text{diag}(\mathbf{w})\mathbf{f}_1\|_1 + \|\text{diag}(\mathbf{w})\mathbf{f}_2\|_1 \\ &\quad \text{s.t. } \mathbf{f}_1 \in \Omega(\mathcal{S}_{\mathcal{V}}, \boldsymbol{\mu}, \boldsymbol{\gamma}), \mathbf{f}_2 \in \Omega(\mathcal{S}_{\mathcal{V}}, \boldsymbol{\gamma}, \boldsymbol{\zeta}) \\ &\geq \min_{\mathbf{f}_1, \mathbf{f}_2 \in \mathbb{R}^{|\mathcal{E}|}} \|\text{diag}(\mathbf{w})\mathbf{f}_1\|_1 + \|\text{diag}(\mathbf{w})\mathbf{f}_2\|_1 \\ &\quad \text{s.t. } \mathcal{S}_{\mathcal{V}}(\mathbf{f}_1 + \mathbf{f}_2) = \boldsymbol{\zeta} - \boldsymbol{\mu} \\ &= \min_{\boldsymbol{\tau}, \boldsymbol{\delta} \in \mathbb{R}^{|\mathcal{E}|}} \|\text{diag}(\mathbf{w})\boldsymbol{\tau} + \boldsymbol{\delta}\|_1 + \|\text{diag}(\mathbf{w})\boldsymbol{\tau} - \boldsymbol{\delta}\|_1 \\ &\quad \text{s.t. } 2\mathcal{S}_{\mathcal{V}}\boldsymbol{\tau} = \boldsymbol{\zeta} - \boldsymbol{\mu} \\ &= \|\text{diag}(\mathbf{w})\hat{\boldsymbol{\tau}} + \hat{\boldsymbol{\delta}}\|_1 + \|\text{diag}(\mathbf{w})\hat{\boldsymbol{\tau}} - \hat{\boldsymbol{\delta}}\|_1 \\ &\geq \|2\text{diag}(\mathbf{w})\hat{\boldsymbol{\tau}}\|_1 \\ &\geq \min_{\mathbf{f} \in \Omega(\mathcal{S}_{\mathcal{V}}, \boldsymbol{\mu}, \boldsymbol{\zeta})} \|\text{diag}(\mathbf{w})\mathbf{f}\|_1 = W_1(\boldsymbol{\mu}, \boldsymbol{\zeta}). \end{aligned} \quad (20)$$

Here, $\boldsymbol{\delta} := 0.5\text{diag}(\mathbf{w})(\mathbf{f}_1 - \mathbf{f}_2)$, $\boldsymbol{\tau} := 0.5(\mathbf{f}_1 + \mathbf{f}_2)$, and

$$\begin{aligned} \hat{\boldsymbol{\tau}}, \hat{\boldsymbol{\delta}} &= \arg \min_{\boldsymbol{\tau}, \boldsymbol{\delta} \in \mathbb{R}^{|\mathcal{E}|}} \|\text{diag}(\mathbf{w})\boldsymbol{\tau} + \boldsymbol{\delta}\|_1 + \|\text{diag}(\mathbf{w})\boldsymbol{\tau} - \boldsymbol{\delta}\|_1 \\ &\quad \text{s.t. } 2\mathcal{S}_{\mathcal{V}}\boldsymbol{\tau} = \boldsymbol{\zeta} - \boldsymbol{\mu}. \end{aligned}$$

In (20), the first inequality is because the number of constraints is reduced and the feasible domain becomes larger. The second inequality leverages the triangular inequality of ℓ_1 -norm. The third inequality is because $2\hat{\boldsymbol{\tau}}$ is a feasible solution corresponding to $W_1(\boldsymbol{\mu}, \boldsymbol{\zeta})$. Replacing \mathcal{V} to a subset of nodes $\mathcal{V}' \subset \mathcal{V}$, we obtain $W_1^{(P)}$ defined on the graph. Based on the same steps, we can prove that $W_1^{(P)}$ is a valid metric in $\text{Range}(\mathcal{S}_{\mathcal{V}'})$. \square

A.2 The Proof of Theorem 2

Proof. Denote $\mathcal{V}_U = \mathcal{V} \setminus \mathcal{V}'$. Based on the shrinkage of the feasible domain, we have

$$\begin{aligned} W_1(\boldsymbol{\mu}, \boldsymbol{\gamma}) &= \min_{\mathbf{f} \in \Omega(\mathcal{S}_{\mathcal{V}}, \boldsymbol{\mu}, \boldsymbol{\gamma})} \|\text{diag}(\mathbf{w})\mathbf{f}\|_1 \\ &= \min_{\mathbf{f} \in \Omega(\mathcal{S}_{\mathcal{V}'}, \boldsymbol{\mu}_{\mathcal{V}'}, \boldsymbol{\gamma}_{\mathcal{V}'}) \cap \Omega(\mathcal{S}_{\mathcal{V}_U}, \boldsymbol{\mu}_{\mathcal{V}_U}, \boldsymbol{\gamma}_{\mathcal{V}_U})} \|\text{diag}(\mathbf{w})\mathbf{f}\|_1 \\ &\geq \min_{\mathbf{f} \in \Omega(\mathcal{S}_{\mathcal{V}'}, \boldsymbol{\mu}_{\mathcal{V}'}, \boldsymbol{\gamma}_{\mathcal{V}'})} \|\text{diag}(\mathbf{w})\mathbf{f}\|_1 = W_1^{(P)}(\boldsymbol{\mu}_{\mathcal{V}'}, \boldsymbol{\gamma}_{\mathcal{V}'}). \end{aligned}$$

The second inequality in (9) can be proven in the same way. The nonnegativeness is based on the metricity. \square

B Experimental Details

B.1 Baseline Implementations and Experimental Settings

All baseline models are implemented using the code released by the respective authors, as provided below.

- **GCN, GAT, APPNP, and BernNet:** <https://github.com/ivam-he/BernNet>
- **ChebNetII:** <https://github.com/ivam-he/ChebNetII>
- **GCN-LPA:** <https://github.com/hwwang55/GCN-LPA>

For GCN, GAT, GIN, GraphSAGE, and APPNP, we search the learning rate over the range of $\{0.001, 0.002, 0.01, 0.05\}$ and the weight decay over the range of $\{0.0, 0.0005\}$. For APPNP, we search its key hyperparameter α over $\{0.1, 0.2, 0.5, 0.9\}$. For BernNet and ChebNetII, we used the hyperparameters provided by the original papers (He et al. 2021, 2022). For GCN-LPA, we apply a two-layer GCN associated with five LPA iteration layers, which follows the settings in (Wang and Leskovec 2021). We utilize the same datasets and data partitioning as BernNet (He et al. 2021) in our experiments.

B.2 Hyperparameter Settings

For all GNN methods, we modify their architectures according to Algorithms 1 and 2 and learn the models through the QW loss. The key hyperparameters and their search spaces are shown below: A_F indicates whether the optimal label transport is involved in the adjustment of edge weights, which is set to True or False. λ is the weights of Bergman divergence, whose search space is $\{10^{-2}, 10^{-1}, \dots, 10^3\}$. lr_F and L_F denote the learning rate and weight decay for the label transport F and MLP-based edge weight predictor. We search for parameter lr_F over the range of $\{0.001, 0.002, 0.01, 0.05\}$ and parameter L_F over the range of $\{0.0, 0.0005\}$.

C Additional Experiments & Analysis

C.1 Comparisons between Algorithms 1 and 2

Additionally, we add more comparisons for Algorithm 1 and Algorithm 2 as shown in Table 6, We can find that the exact solver (Algorithm 2) works well on homophilic graphs while the inexact solver (Algorithm 1) works well on some challenging heterophilic graphs in GCN and APPNP. This may be empirical evidence for selecting the algorithms. However, it is worth noting that there is not such a clear pattern for other models, as mentioned in the Remark. In practice, we select solvers based on the performance.

Table 6: Comparisons of Algorithm 1 and Algorithm 2 on node classification accuracy (%).

Model	Method	Cora	Citeseer	Pubmed	Computers	Photo	Squirrel	Chameleon	Actor	Texas	Cornell
GCN	(2)	87.44 \pm 0.96	79.98 \pm 0.84	86.93 \pm 0.29	88.42 \pm 0.45	93.24 \pm 0.43	46.55 \pm 1.15	63.57 \pm 1.16	34.00 \pm 1.28	77.21 \pm 3.28	61.91 \pm 5.11
	Algorithm1	86.95 \pm 1.12	81.30 \pm 0.37	87.89 \pm 0.44	88.39 \pm 0.55	93.80 \pm 0.37	51.04 \pm 0.51	67.77 \pm 0.92	38.09\pm0.50	84.10\pm2.95	84.26\pm2.98
	Algorithm2	87.88\pm0.79	81.36\pm0.41	87.89\pm0.40	89.20\pm0.41	93.81\pm0.36	52.62\pm0.49	68.10\pm1.01	31.36 \pm 0.84	78.03 \pm 2.13	67.23 \pm 4.04
APNP	(2)	88.33 \pm 0.77	81.28\pm0.71	88.62 \pm 0.33	86.27 \pm 0.37	93.70 \pm 0.27	36.15 \pm 0.75	52.93 \pm 1.71	40.46 \pm 0.64	91.31 \pm 1.97	87.66 \pm 2.31
	Algorithm1	88.69 \pm 1.00	80.94 \pm 0.61	89.39 \pm 0.31	86.85 \pm 0.73	93.25 \pm 0.38	37.11 \pm 0.60	53.76\pm1.25	40.78\pm0.74	91.48\pm1.80	87.87\pm2.34
	Algorithm2	88.74\pm0.84	80.71 \pm 0.50	89.48\pm0.28	86.95\pm0.82	94.43\pm0.24	38.73\pm1.06	53.54 \pm 1.51	40.53 \pm 0.63	91.31 \pm 1.48	87.23 \pm 2.77

Table 7: Comparisons of different models on node classification accuracy (%).

Model	Method	Cora	Citeseer	Pubmed	Photo	Squirrel	Chameleon
Train		140	120	60	160	100	100
Valid		500	500	500	500	500	500
Test		1000	1000	1000	1000	1000	1000
GCN	(2)	79.50 \pm 0.81	69.73\pm0.61	81.70 \pm 0.80	91.49 \pm 0.62	29.29 \pm 1.51	45.72 \pm 1.65
	QW	79.83\pm1.11	69.32 \pm 0.77	81.81\pm0.62	92.01\pm0.67	30.02\pm0.90	50.78\pm1.15
GAT	(2)	80.86 \pm 0.83	69.57 \pm 0.78	81.48\pm1.02	91.33 \pm 0.40	26.21 \pm 1.09	47.03 \pm 2.10
	QW	81.01\pm0.93	69.64\pm0.59	81.27 \pm 0.82	92.07\pm0.44	28.35\pm1.34	48.50\pm1.32

C.2 More Data-Splitting Setting Comparisons

As shown in Figure 4, we present the experimental results with training set percentages of 1%, 5%, 10%, 20%, 30%, 40%, 50%, and 60%. To further validate robustness, we conducted extra experiments with a data-splitting strategy: 20 nodes/class for training, 500 nodes for validation, and 1000 nodes for testing. The results are shown in Table 7. We can find that under the same data-splitting setting, applying QW loss can still improve the model performance in most situations. In particular, even if the number of labeled training nodes is significantly smaller than that of testing nodes, for homophilic graphs, the performance of applying our QW loss is at least comparable to that of the traditional method (i.e., (2)). Moreover, for heterophilic graphs, our QW loss leads to significant improvements.

C.3 More Analysis on Model Parameters

Because of learning the optimal flow matrix F , whose size is $|\mathcal{E}| \times C$, our method involves more model parameters. However, in Table 8, we demonstrate that the improvements achieved by our QW loss are attributed to the rationality of the loss function and associated transductive learning paradigm, rather than merely increasing model parameters. We increase the model parameter of GAT (by adding their layer width and/or depth), making the model size comparable to ours. The experimental results below show that even with a similar model size, applying QW loss leads to better model performance. In essence, the improvements achieved by QW loss are at least not merely from over-parametrization.

C.4 More Analysis on Learnable Edge Weights

As shown in Table 5, adjusting edge weights based on F^* leads to better accuracy for the GCN on heterophilic graphs. In our opinion, this phenomenon is reasonable. The performance of a GNN on a graph is determined by three factors: (a) the rationality of training loss, (b) the expressivity of GNN, and (c) the hardness of data. Our QW loss focuses on (a). For the GNN with limited expressivity, i.e., the GCN, adjusting edge weights based on our flow matrix can naturally enhance its representation power. However, for ChebNetII, the model itself has already been able to achieve

Table 8: Comparisons under different training parameter numbers on Squirrel and Pubmed.

Loss	Squirrel			Pubmed		
	Setting	#Para.	Acc.	Setting	#Para.	Acc.
CE	hidden dim.=64	1,073,679	48.20 \pm 1.67	hidden dim.=64	259,081	87.42 \pm 0.33
	hidden dim.=125	2,097,015	48.72 \pm 1.59	hidden dim.=100	404,809	87.49 \pm 0.36
	hidden dim.=128	2,147,343	49.18 \pm 1.67	hidden dim.=128	518,153	87.49 \pm 0.28
	hidden dim.=125 #head=5 #layer=3	2,202,639	44.74 \pm 0.74	hidden dim.=112 #head=4 #layer=3	428,745	86.08 \pm 0.43
QW	hidden dim.=64	2,065,444	55.03 \pm 1.35	hidden dim.=64	392,053	88.38 \pm 0.23

various spectral filters, so we do not have to further adjust edge weights. Finally, the nodes in a heterophilic graph often have different labels compared to their neighbors. Therefore, the flow matrix captures the necessary label transport among the nodes, and adjusting edge weights accordingly introduces useful information for the GNN. In summary, adjusting weights is useful for simple GNNs, especially when learning them on heterophilic graphs.

C.5 Minor Improvements on Several Datasets

In Table 2, the improvements achieved by our QW loss are incremental for homophilic graphs while significant for heterophilic graphs. In our opinion, the potential reason for this phenomenon is the different difficulties of the learning tasks and the nature of label transportation flow. In a homophilic graph, the label of a node is often the same as those of its neighbors. As a result, a simple low-pass filter-like GNN can predict the labels with high accuracy, and the residual between the GNN’s output and the observed labels, i.e., \mathbf{SF}^* , is small. According to (18), when \mathbf{SF}^* is small, it has little impact on the prediction results. Therefore, the improvements achieved by QW loss are limited for homophilic graphs.

On the contrary, in a heterophilic graph, the label of a node is often different from those of its neighbors, and thus the learning tasks become much harder — the prediction of the neighbors might be useless for the prediction of the central node, and the central node needs to leverage the information from the nodes far away from it, which is achieved by the label transportation flow in the shortest paths. In such a situation, it is challenging to learn a GNN to predict the labels with high accuracy, and the complementary information provided by becomes necessary and effective. Additionally, as shown in Figure 4, when the learning task is difficult enough, e.g., training a node classifier based on sparse labels, applying our QW loss consistently outperforms the traditional learning method on both homophilic and heterophilic graphs, with significant improvements. A potential reason for this phenomenon is that given sparse labels, the GNN often suffers from the over-fitting issue. In such a situation, \mathbf{SF}^* provides additional information from observed labels, which may help to improve prediction accuracy.